Frequency Comparison of Two High-Accuracy Al^+ Optical Clocks

C. W. Chou,* D. B. Hume, J. C. J. Koelemeij,† D. J. Wineland, and T. Rosenband

Time and Frequency Division, National Institute of Standards and Technology, Boulder, Colorado 80305, USA

(Received 23 November 2009; published 17 February 2010)

We have constructed an optical clock with a fractional frequency inaccuracy of 8.6×10^{-18}, based on quantum logic spectroscopy of an Al^+ ion. A simultaneously trapped Mg^+ ion serves to sympathetically laser cool the Al^+ ion and detect its quantum state. The frequency of the $^1S_0 \leftrightarrow {}^3P_0$ clock transition is compared to that of a previously constructed Al^+ optical clock with a statistical measurement uncertainty of 7.0×10^{-18}. The two clocks exhibit a relative stability of $2.8 \times 10^{-15}\tau^{-1/2}$, and a fractional frequency difference of -1.8×10^{-17}, consistent with the accuracy limit of the older clock.

DOI: 10.1103/PhysRevLett.104.070802 PACS numbers: 06.20.F−

Optical clocks based on petahertz (10^{15} Hz) transitions in isolated atoms have demonstrated significant improvements over the current cesium primary frequency standards at 9.2 GHz. They also shed light on fundamental physics, such as the possible variation of physical constants. While the merits of laser cooled ion optical frequency standards were known [1,2], further developments were required to permit their use. Subhertz linewidth lasers [3] enabled single ions to be probed with sufficient resolution for high-stability clock operation, and control of external-field perturbations allowed such clocks to operate with an inaccuracy below 10^{-16} [4,5]. For comparison, cesium standards that realize the SI second have reached an inaccuracy of 3×10^{-16} [6], and an optical lattice clock based on Sr atoms has been reported [7] with an inaccuracy of 1.5×10^{-16}. Here we describe an Al^+ ion clock with an inaccuracy of 8.6×10^{-18}.

The $^1S_0 \leftrightarrow {}^3P_0$ transition in Al^+ at 1.121 PHz is of interest due to its low sensitivity to electromagnetic perturbations and its narrow natural linewidth of 8 mHz [8,9]. Al^+ has the smallest sensitivity to blackbody radiation [10,11] among atomic species currently under consideration for clocks, thus relaxing the requirement on ambient temperature control. However, the absence of an accessible allowed optical transition prevents the internal state of Al^+ ions from being detected by conventional methods, and the ion cannot currently be directly laser cooled. Quantum logic spectroscopy (QLS) [12] overcomes these difficulties by trapping a "logic ion" that can be directly laser cooled together with the Al^+ clock ion. The coupled motion of the two ions allows for sympathetic cooling, as well as the transfer of the clock ion's quantum state to the logic ion, where the state can be measured.

The clock described here shares features with our previously-constructed Al-Be clock [5,9], but also includes many changes, making a comparison of the two clocks a valuable test of systematic errors. In the new clock, the $^9Be^+$ logic ion has been replaced by $^{25}Mg^+$, whose mass closely matches that of $^{27}Al^+$. Laser cooling inefficiencies due to mass mismatch are thus suppressed. The Al-Mg ion trap is a linear Paul trap built from tool machined all-metal electrodes (Fig. 1). This construction differs from the Al-Be trap that was built from laser-machined and gold-coated alumina electrodes [13], and it exhibits reduced rf-micromotion-inducing electric fields.

QLS with a Mg^+ logic ion proceeds in the same way as with Be^+, but the ground-state-cooling process [14] has been modified to require only two lasers rather than three [15]. This cools the out-of-phase axial motional mode to an average quantum number of $\bar{n} < 0.05$. It also enables quantum-nondemolition transfer (QNDT) of the Al^+-clock-ion state to Mg^+ with approximately 80% fidelity in a single QNDT repetition and over 99% fidelity after typically five QNDT repetitions [16].

The trap utilized in the new Al^+ clock has blade-shaped gold-coated beryllium-copper electrodes (Fig. 1) whose edges are approximately 400 μm from the ions. The $^{25}Mg^+$ logic ion ($I = 5/2$) is manipulated with light of 279.5 nm wavelength from two independent lasers. A frequency doubled dye laser resonantly drives

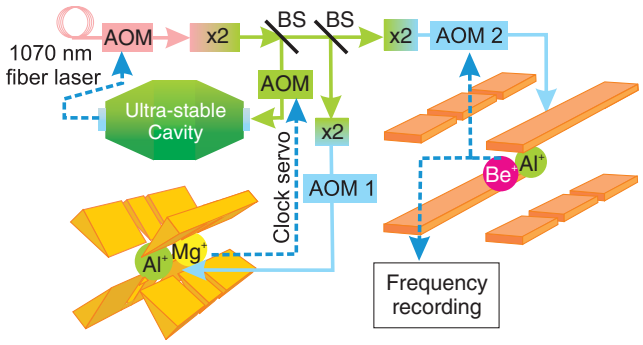

FIG. 1 (color). Setup for comparing the frequencies of the two Al^+ clocks. The 4th harmonic of a fiber laser is locked to the Al^+ $^1S_0 \leftrightarrow {}^3P_0$ clock transition in the Al-Mg apparatus with a fixed offset frequency (applied to AOM1). Another laser beam derived from the same laser probes the clock transition in the Al-Be apparatus, where the laser frequency is locked to the clock transition in a separate digital feedback loop that controls AOM2. The record of frequencies applied to AOM2 represents the difference in clock frequencies. Beam splitter (BS); acousto-optic modulator (AOM); frequency doubler (x2).

$|^2S_{1/2}, F \in \{2, 3\}\rangle \rightarrow {}^2P_{3/2}$ cycling and repumping transitions, while a frequency-quadrupled fiber laser is detuned by 40–60 GHz to drive Raman transitions between the $^{25}Mg^+$ hyperfine qubit states. Both ions are created via multiphoton ionization of neutral atoms from ovens. A 396 nm diode laser produces $^{27}Al^+$ [17], while a frequency-doubled dye laser at 285 nm creates $^{25}Mg^+$ [18]. Typically the clock transition is probed with 150 ms duration π pulses with a duty cycle of approximately 65%. The remaining 35% is occupied with state preparation and state detection functions as well as interleaved experiments that allow real-time measurement and reduction of micromotion.

Systematic shifts of the Al-Mg clock are listed in Table I. Two types of residual motion cause time-dilation shifts: micromotion near the trap drive frequency of $\nu_{\mathrm{rf}} = 59$ MHz, and harmonic-oscillator (secular) motion at the ion's normal mode frequencies (Table II). In both cases the clock frequency shifts by $\frac{\Delta\nu}{\nu} = -\frac{\langle v^2\rangle}{2c^2}(1 + (\frac{f}{400\ \mathrm{MHz}})^2)$, where we add to the relativistic time-dilation $\langle v^2\rangle/(2c^2)$ a frequency-dependent term that corresponds to the Stark shift from the motion-inducing electric fields. Here $\langle v^2\rangle$ is the mean-squared Al^+-ion velocity and f is the frequency of motion. For the highest motional frequencies the Stark shift correction is 2%.

Excess micromotion (EMM) refers to the rapid ion motion at ν_{rf} [19]. It is caused by electric fields that force the ion away from the rf minimum of the ion trap, or phase shifts between trap electrodes that cause the rf fields to be nonzero at the pseudopotential minimum. We measure the amplitude of this motion at ν_{rf} by observing the motional-sideband strength of the Al^+ $^1S_0 \rightarrow {}^3P_1$ transition in three orthogonal directions. For small amplitude of motion, the time-dilation shift is $\Delta\nu/\nu = -|\vec{\eta}\nu_{\mathrm{rf}}/\nu_L|^2 = -2.8 \times 10^{-15}|\vec{\eta}|^2$, where $\nu_L \approx 1.12$ PHz is the probe laser frequency, and $\vec{\eta} = (\eta_1, \eta_2, \eta_3)$ is the measured EMM Lamb-Dicke parameter (the ratio of sideband and carrier Rabi rates) for the three orthogonal directions. Typical values for $\eta_{1,2,3}$ are 0.01 to 0.04. We note that this EMM measurement method detects slow electric field fluctuations such as those caused by the migration of photoelectrons, as well as faster fluctuations caused by periodic line noise (50 to 60 Hz). Fluctuations that are shorter than the laser probe period of 0.05 to 0.1 ms will not be detected.

TABLE I. Systematic effects that shift the clock from its ideal unperturbed frequency. Shifts and uncertainties given are in fractional frequency units ($\Delta\nu/\nu$). See text for discussion.

Effect	Shift (10^{-18})	Uncertainty (10^{-18})
Excess micromotion	−9	6
Secular motion	−16.3	5
Blackbody radiation shift	−9	3
Cooling laser Stark shift	−3.6	1.5
Quad. Zeeman shift	−1079.9	0.7
Linear Doppler shift	0	0.3
Clock laser Stark shift	0	0.2
Background-gas collisions	0	0.5
AOM freq. error	0	0.2
Total	−1117.8	8.6

In a perfect linear Paul trap EMM along the trap axis does not occur, but imperfections in the ion-trap geometry can lead to axial EMM. For the Al-Mg trap there exists a sharp minimum of axial EMM at one spatial location. The Al^+ ion is held at this point, but random background-gas collisions cause the Al-Mg ion pair to spontaneously reorder, which causes the Al^+ ion to move by 3 μm every 200 s, on average. The Al^+ ion is maintained at the position of minimal micromotion by adjusting the electrode voltages every 10 s to force the ion pair into the desired order. When the ions are in the wrong order (about 5% of the time), the Al^+ ion experiences excess axial micromotion and a corresponding clock shift of $\Delta\nu/\nu = -2.7 \times 10^{-17}$. This additional shift is included in Table I.

During each Al^+ clock interrogation pulse, the Mg^+ ion is simultaneously Doppler cooled by a laser that is tuned 21 MHz below the $|^2S_{1/2}, F = 3, m = -3\rangle \rightarrow |^2P_{3/2}, F = 4, m = -4\rangle$ cycling transition. The amplitude of secular motion (corresponding to the motional temperature) is extracted from the ratio of amplitudes for the red and blue sidebands of a Raman transition for all six normal modes [14]. Measured values are shown in Table II, together with values calculated from laser cooling theory for a single ion [20]. The single-Mg^+-ion Doppler cooling limit is also valid when applied to each of the six normal modes of the Al-Mg ion pair. The measured and calculated motional quantum numbers agree within the measurement uncertainty, and we consider the stated 30% uncertainty for this shift to be a conservative limit.

The Mg^+ Doppler cooling laser beam maintains the Al-Mg ion pair at a constant motional temperature during the clock interrogation pulse, but because it also overlaps the Al^+ ion, it causes an ac Stark shift by coupling off-resonantly to allowed transitions that connect to the ground $(3s^2)^1S_0$ and excited $(3s3p)^3P_0$ clock states. Following the evaluation of the blackbody radiation shift [10], we estimate the differential clock polarizability at 279.5 nm as $\Delta\nu/\nu = (-3.5 \pm 0.6) \times 10^{-17}S$, where $S(= I/I_S)$ is the saturation parameter for $^{25}Mg^+$ ($I_S \approx 2470\ \mathrm{W/m^2}$). The intensity I of the Mg^+ Doppler cooling laser is estimated from the rate at which this laser repumps the $|^2S_{1/2}, F = 2, m = -2\rangle$ dark hyperfine ground state. The ion fluorescence photomultiplier counts $F(t)$ collected in a duration t due to repumping of the dark state may be written as $F(t) = b(t + \tau(e^{-t/\tau} - 1))$ where $\tau = (0.217/S)$ ms and b is the bright-state counting rate. We extract S by fitting $F(t)$ to the observed ion fluorescence. Typically, we measure $\tau = 2.1 \pm 0.8$ ms, and find $\Delta\nu/\nu = (-3.6 \pm 1.5) \times 10^{-18}$.

Another Stark shift is caused by thermal blackbody radiation. The temperature of the Al-Mg ion trap is mea-

TABLE II. Motional modes of the Al-Mg ion pair. For each of the six normal modes, the oscillation frequency and zero-point motional amplitude for each ion is listed. The trap axis corresponds to $\hat{z}$, and $\hat{x}$, $\hat{y}$ are two orthogonal radial directions whose orientation is determined by the trap geometry. Also shown are the calculated ($\bar{n}_C$) and measured ($\bar{n}_M$) Doppler-cooled average motional quantum numbers, and the time-dilation (TD) per motional quantum as well as the total TD per mode.

f [MHz]	6.53	5.66	5.20	4.64	3.41	3.00
$^{25}Mg^+$ [nm]	$4.9\hat{y}$	$2.9\hat{y}$	$4.6\hat{z}$	$5.5\hat{x}$	$-4.2\hat{x}$	$5.6\hat{z}$
$^{27}Al^+$ [nm]	$2.6\hat{y}$	$-5.0\hat{y}$	$-4.1\hat{z}$	$3.5\hat{x}$	$6.2\hat{x}$	$5.8\hat{z}$
$\bar{n}_M$	2.9	4.5	3.4	6.3	10.0	7.0
$\bar{n}_C$	3.3	3.8	3.4	5.9	8.0	5.9
TD/quantum [10^{-18}]	0.226	0.731	0.197	0.290	0.771	0.133
Total TD [10^{-18}]	0.77	3.66	0.77	1.97	8.10	1.00

sured with two platinum sensors at opposite ends of the trap structure which are expected to be at temperature extremes. Heat is removed primarily through thermal conduction at one end of the trap where we measure a temperature of 35 °C. At the higher thermal resistance trap-end the temperature is 40 °C, and the thermal radiation field impinging upon the ion is bounded by this maximum temperature and the laboratory room temperature of 22 °C: $T_{\mathrm{ion}} = (31 \pm 9)$ °C.

During operation, the Al^+ clock servo alternates between probing of the $|^1S_0, m_F = 5/2\rangle \leftrightarrow |^3P_0, m_F = 5/2\rangle$ and $|^1S_0, m_F = -5/2\rangle \leftrightarrow |^3P_0, m_F = -5/2\rangle$ transitions every 5 s, and the apparatus synthesizes an average of these two frequencies to eliminate first-order Zeeman shifts [9,21]. Each transition's resonance is probed several times at the high- and low-frequency half-maximum points to derive a frequency-correction signal. The frequency difference between the transitions is proportional to the mean magnetic field $\langle B \rangle$, which allows an accurate estimate of the quadratic Zeeman shift due to the quasistatic quantization field of typically $\langle B \rangle = 0.1$ mT. However, the quadratic Zeeman shift is proportional to $\langle B^2 \rangle = \langle B \rangle^2 + B_{\mathrm{ac}}^2$, where B_{ac}^2 is the variance of the magnetic field about its mean. The dominant sources of varying magnetic fields are currents at ν_{rf} in conductors near the ion. We vary the trap rf drive power P and measure the frequency of the hyperfine clock transition in $^{25}Mg^+$ $|F = 3, m_F = 0\rangle \rightarrow |F = 2, m_F = 0\rangle$ near 1.789 GHz, which has a strong quadratic dependence on the magnetic field, to find $B_{\mathrm{ac}}^2 = 1.45 \times 10^{-12}\ (\mathrm{P/W})\ \mathrm{T}^2$. For Al^+ clock operation $P = 15$ W, and $B_{\mathrm{ac}}^2 = 2.17 \times 10^{-11}\ \mathrm{T}^2$, which alters the quadratic Zeeman shift by $\Delta\nu/\nu = (-1.4 \pm 0.3) \times 10^{-18}$.

Other potential systematic shifts are listed in Table I. When stabilizing the clock laser to the ion we probe the clock transition alternately with counterpropagating laser beams to observe and cancel potential first-order Doppler shifts [5]. For the clock comparison described below, we observe a differential shift for the two probe directions of $(1.2 \pm 0.7) \times 10^{-17}$ but this effect is suppressed by taking the average. The suppression factor is limited because the atomic line shape and hence the servo gains differ slightly for the two probe directions. During clock operation the mean fractional gain imbalance was 1.5%, thereby reducing the possible first-order Doppler shift to 3×10^{-19}.

We have looked for Stark shifts due to the clock pulse itself by raising the intensity of the probe beam in one clock, and comparing the frequency to that produced by the other Al^+ clock. With an increase of 40 dB in the clock probe intensity, we observe no statistically significant frequency difference with a fractional uncertainty of 2×10^{-15}, constraining any effect that scales linearly with this intensity to 2×10^{-19}. We observe a rate of background-gas collisions similar to the Al-Be clock and assign a 5×10^{-19} uncertainty to this potential shift [5]. Thermally induced frequency errors from beam switching AOMs (Fig. 1) have been evaluated previously [5], and this uncertainty is reduced to 2×10^{-19} by operating the AOMs at less than 1 mW.

We directly compared the Al-Mg clock with the Al-Be clock to perform independent tests that could reveal unaccounted-for clock shifts. The Al-Be clock was evaluated with an accuracy of 2.3×10^{-17} [5], and this evaluation remained valid during the two-clock comparison. The two clocks were compared in 56 separate measurements, each of duration 1000–11 000 s. As shown in Fig. 1, the frequency of the $^1S_0 \leftrightarrow {}^3P_0$ probe laser was actively steered to the Al^+ ion in the Al-Mg apparatus with a servo time-constant of about 10 s. A portion of this laser light simultaneously probed the Al^+ ion in the Al-Be clock, where it was servoed to the clock transition in a separate digital feedback loop. The frequency produced by this feedback loop represents the frequency difference between the two clocks, and was recorded and analyzed for stability (Fig. 2). Average frequencies of the individual measurements corrected for known shifts are shown in Fig. 3, where the overall weighted mean is $(\nu_{\mathrm{AlMg}} - \nu_{\mathrm{AlBe}})/\nu = (-1.8 \pm 0.7) \times 10^{-17}$. This value is consistent with the 1-σ error of 2.5×10^{-17} that is calculated by adding in quadrature the inaccuracies of the two clocks and the statistical uncertainty. The reduced-χ^2 for this data set is 1.02, indicating that the error bars derived from the estimated stability correctly capture the scatter of the data. For this data set the total in-loop servo error for the Al-Mg clock was $\Delta\nu/\nu = 6 \times 10^{-19}$, and for a well-designed servo loop this error declines faster than the

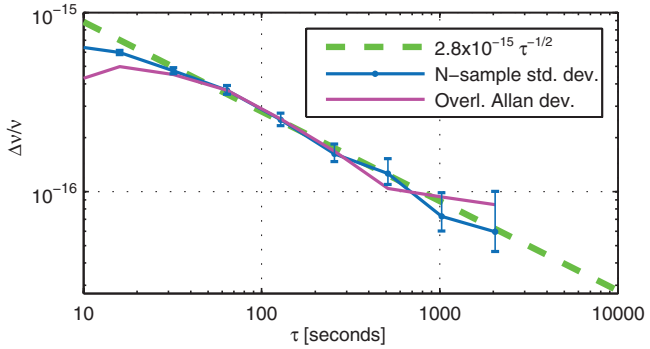

FIG. 2 (color). Clock stability. Fractional frequency uncertainty vs averaging period (τ) for a comparison between the two Al^+ clocks (10 700 s duration). Overlapping Allan deviation and N-sample standard deviation are shown [24]. For each comparison measurement the coefficient of the $\tau^{-1/2}$ asymptote is estimated and used to derive the measurement's statistical uncertainty. The $2.8 \times 10^{-15}\tau^{-1/2}$ asymptote is reached for averaging periods that are longer than the servo time constant of 10 s.

statistical error. It is therefore not included as a systematic shift in Table I.

In summary, we have built an Al^+ ion clock with a fractional frequency inaccuracy of 8.6×10^{-18}. Its frequency is compared to that of a previously constructed Al^+ clock, and the measured fractional frequency difference of $(-1.8 \pm 0.7) \times 10^{-17}$ is consistent with the inaccuracy of the previous clock. Significantly, the statistical uncertainty in the frequency comparison of 7.0×10^{-18} is smaller than the inaccuracy of either clock, and the average measurement stability was $2.8 \times 10^{-15}\tau^{-1/2}$ (total measurement duration: 164 967 s). This result may be compared to other direct same-species atomic clock comparisons, where two Cs microwave clocks have reached an agreement of $(4 \pm 3) \times 10^{-16}$ [22], and two Yb^+ single ion clocks showed agreement of $(3.8 \pm 6.1) \times 10^{-16}$ [23].

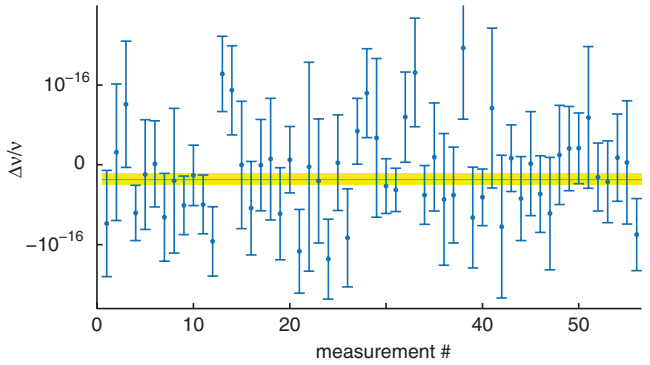

FIG. 3 (color). Measurements of the fractional frequency difference between the two Al^+ clocks (blue points). Error bars represent the statistical uncertainty (see Fig. 2). The horizontal line shows the weighted mean of -1.8×10^{-17} with an overall statistical uncertainty of $\pm 7.0 \times 10^{-18}$ (shaded band).

Future frequency ratio measurements of the Al^+ clock and the NIST Hg^+ optical clock would enable improved constraints on present-era changes in the fine-structure constant [5].

We thank J. C. Bergquist for use of his stable Fabry-Perot cavities, T. M. Fortier for optical frequency measurements, W. M. Itano for atomic structure calculations, and S. Bickman and D. Leibrandt for helpful comments on the manuscript. This work was supported by ONR. J. C. J. K. acknowledges support from the Netherlands Organisation for Scientific Research (NWO). Contribution of NIST, not subject to U.S. copyright.

*chinwen@nist.gov
†Present address: Laser Centre Vrije Universiteit Amsterdam, The Netherlands.

[1] H. G. Dehmelt, IEEE Trans. Instrum. Meas. **IM-31**, 83 (1982).
[2] D. J. Wineland, W. M. Itano, J. C. Bergquist, and R. G. Hulet, Phys. Rev. A **36**, 2220 (1987).
[3] B. C. Young, F. C. Cruz, W. M. Itano, and J. C. Bergquist, Phys. Rev. Lett. **82**, 3799 (1999).
[4] W. H. Oskay *et al.*, Phys. Rev. Lett. **97**, 020801 (2006).
[5] T. Rosenband *et al.*, Science **319**, 1808 (2008).
[6] T. E. Parker, Metrologia **47**, 1 (2010).
[7] G. K. Campbell *et al.*, Metrologia **45**, 539 (2008).
[8] N. Yu, H. Dehmelt, and W. Nagourney, Proc. Natl. Acad. Sci. U.S.A. **89**, 7289 (1992).
[9] T. Rosenband *et al.*, Phys. Rev. Lett. **98**, 220801 (2007).
[10] T. Rosenband *et al.*, arXiv:physics/0611125.
[11] J. Mitroy, J. Y. Zhang, M. W. J. Bromley, and K. G. Rollin, Eur. Phys. J. D **53**, 15 (2009).
[12] P. O. Schmidt *et al.*, Science **309**, 749 (2005).
[13] M. A. Rowe *et al.*, Quantum Inf. Comput. **2**, 257 (2002).
[14] C. Monroe *et al.*, Phys. Rev. Lett. **75**, 4011 (1995).
[15] The entropy-reducing laser that repumps the states $|^2S_{1/2}, F \in \{2, 3\}, m = -2\rangle$ via $|^2P_{1/2}, F = 3, m = -3\rangle$ into $|^2S_{1/2}, F = 3, m = -3\rangle$ is replaced by the repeated application of a pulse sequence that first drives the $|^2S_{1/2}, F = 2, m = -2\rangle \rightarrow |^2P_{3/2}, F = 3, m = -3\rangle$ transition and, subsequently, the transition $|^2S_{1/2}, F = 3, m = -2\rangle \rightarrow |^2S_{1/2}, F = 2, m = -2\rangle$.
[16] D. B. Hume, T. Rosenband, and D. J. Wineland, Phys. Rev. Lett. **99**, 120502 (2007).
[17] G. S. Hurst, M. G. Payne, S. D. Kramer, and J. P. Young, Rev. Mod. Phys. **51**, 767 (1979).
[18] N. Kjaergaard *et al.*, Appl. Phys. B **71**, 207 (2000).
[19] D. J. Berkeland *et al.*, J. Appl. Phys. **83**, 5025 (1998).
[20] W. M. Itano and D. J. Wineland, Phys. Rev. A **25**, 35 (1982).
[21] J. E. Bernard, L. Marmet, and A. A. Madej, Opt. Commun. **150**, 170 (1998).
[22] C. Vian *et al.*, IEEE Trans. Instrum. Meas. **54**, 833 (2005).
[23] T. Schneider, E. Peik, and C. Tamm, Phys. Rev. Lett. **94**, 230801 (2005).
[24] W. J. Riley, *NIST Special Publication 1065* (NIST, Boulder, CO, 2008).